Variational quantum process tomography of two-qubit maps

Reinaldo O. Vianna,[1] Andrea Crespi,[2,3] Roberta Ramponi,[2,3] Roberto Osellame,[2,3] Linda Sansoni,[4,*] Giorgio Milani,[4] Paolo Mataloni,[4,5] and Fabio Sciarrino[4,5]

[1]*Departamento de Física-ICEx-Universidade Federal de Minas Gerais, Avenida Presidente Antônio Carlos 6627, Belo Horizonte, Minas Gerais 31270-901, Brazil*

[2]*Istituto di Fotonica e Nanotecnologie, Consiglio Nazionale delle Ricerche (IFN-CNR), Piazza Leonardo da Vinci, 32, I-20133 Milano, Italy*

[3]*Dipartimento di Fisica, Politecnico di Milano, Piazza Leonardo da Vinci, 32, I-20133 Milano, Italy*

[4]*Dipartimento di Fisica, Sapienza Università di Roma, Piazzale Aldo Moro, 5, I-00185 Roma, Italy*

[5]*Istituto Nazionale di Ottica, Consiglio Nazionale delle Ricerche (INO-CNR), Largo Enrico Fermi, 6, I-50125 Firenze, Italy*

(Received 7 November 2012; published 6 March 2013)

Full characterization of quantum states and processes is a fundamental requirement for verification and benchmarking of quantum devices. It has been realized in systems with few components, but for larger systems it becomes unfeasible because of the exponential growing with the system size of the number of measurements and the amount of computational power required to process them. A new approach for quantum state tomography and quantum process tomography, requiring a limited number of measurements, has been recently introduced by Maciel *et al.* [Quantum Inf. Comput. **12**, 0442 (2012); Int. J. Mod. Phys. C **22**, 1361 (2011).], namely variational quantum-process tomography (VQT). Here we adopt the VQT approach for the experimental characterization of two-qubit quantum processes and compare the reconstructed maps with those obtained by standard tomographic methods. The results demonstrate the high performance of this approach and propose VQT as a powerful alternative to the standard quantum process tomography.

DOI: 10.1103/PhysRevA.87.032304 PACS number(s): 03.67.Pp, 03.65.Wj

I. INTRODUCTION

In order to make feasible quantum information processing, an efficient characterization of quantum processing elements is necessary. A completely positive map can be described by a linear operator: The experimental characterization of this operator, taking the name of quantum process tomography (QPT) [1–3], is a very helpful tool, for instance, to design appropriate quantum error correcting codes [4].

Although QPT provides a full characterization of any quantum operation, in general, the reconstruction of the process matrix is a challenging task. The amount of parameters involved, in fact, scales exponentially with the number of qubits and is proportional to $D^4 - D^2$, where $D = 2^n$ for a system of n qubits. Hence, the estimation of such parameters requires an exponentially growing number of measurements. To overcome these experimental limitations, different methods have been proposed to estimate quantum states and processes with a polynomially growing amount of measurements [5–11]. The present work is part of this larger effort to try to make quantum tomography more efficient through the use of shortcuts that are then justified by the data.

Here we exploit the variational quantum process tomography (VQT) introduced by Maciel *et al.* [12,13]: It is a linear convex optimization problem based on semidefinite programs (SDP) [14] which can be solved very efficiently by means of interior point algorithms [15]. A paramount characteristic of the method is given by its ability to accomplish the process tomography using partial information, like in MaxEnt approaches [16,17]. Another outstanding characteristic of VQT is given by its convergence property similar to the compressed sensing approach introduced by Gross *et al.* [5], namely, a faithful reconstruction of a quantum state with cost $O(rd \ln d)$, where d is the dimension of the Hilbert (Hilbert-Schmidt) space and r is the rank of the state (process). VQT was previously tested for the tomography of quantum states in both a quantum optics experiment [18] and a NMR experiment [19]. A general and in-depth discussion about the VQT is given in Refs. [12,13], where the method was numerically tested for different bases and measurement errors. We note that the ability of VQT to accomplish the process tomography using partial information, together with the high efficiency in solving linear convex optimization problems, makes this new method promising for analyzing quantum processes of many qubits.

In order to benchmark the VQT approach for the reconstruction of quantum processes we choose to characterize a two-qubit gate which represents one of the building blocks of quantum computation, i.e., the controlled-NOT (CNOT) gate. To this purpose we fully analyze the quantum operation implemented by the integrated CNOT gate recently realized by Crespi *et al.* [20], using the VQT approach. We explore the peculiar features of this method to investigate the performances of the quantum gate on different input states, concluding for its stability and high fidelity. This study completes the first process tomography characterization performed in Ref. [20], using the *maximum likelihood* approach of Bongioanni *et al.* [3]. This work represents an application of the VQT method to study an experimental process tomography.

II. CNOT GATE FOR POLARIZATION QUBITS

Universal quantum computation may be achieved by using single-qubit transformations and two-qubit gates [21]. The most commonly exploited two-qubit gate is the CNOT which flips the target qubit (T) depending on the state of the control qubit (C). The CNOT action is described by a unitary

*linda.sansoni@gmail.com

 ©2013 American Physical Society

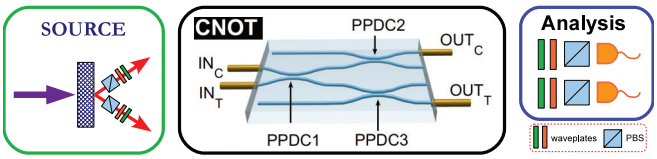

FIG. 1. (Color online) Scheme of the experimental setup of Ref. [20]. Pairs of entangled photons are generated via spontaneous parametric down-conversion in a nonlinear crystal (left) and injected in the integrated CNOT gate. Standard analysis setups are adopted to perform quantum state tomography of the outcoming photons (right).

transformation acting on a generic superposition of two-qubit quantum states. In the computational basis $\{|00\rangle,|01\rangle,|10\rangle,|11\rangle\}$ for the systems C and T, the CNOT matrix reads

$$\mathcal{U}_{\text{CNOT}} = \begin{pmatrix} 1 & 0 & 0 & 0 \\ 0 & 1 & 0 & 0 \\ 0 & 0 & 0 & 1 \\ 0 & 0 & 1 & 0 \end{pmatrix}. \tag{1}$$

The simplest scheme to implement a CNOT for polarization-encoded qubits exploits three partial polarizing beam splitters (PPBSs) with suitable polarization-dependent transmittivities [22,23]. The two-photon interaction occurs by a Hong-Ou-Mandel effect [24] in a single PPBS, while the other two PPBSs operate as compensators. Such a scheme has been experimentally implemented by using bulk optics [25–28] or fiber couplers [29].

In this context, an important step forward in the development of quantum information technology has been given by Crespi *et al.* [20], with the implementation of the first integrated photonic CNOT gate for polarization-encoded qubits. The integrated CNOT is achieved by the optical scheme given in Fig. 1 (center): It consists of a first partially polarizing directional coupler (PPDC1)—the integrated device corresponding to a bulk PPBS—with transmittivities $T_H^{(1)} = 0$ and $T_V^{(1)} = \frac{2}{3}$, where target and control qubits interfere, followed by two other directional couplers (PPDC2 and PPDC3), with $T_H^{(2,3)} = \frac{1}{3}$ and $T_V^{(2,3)} = 1$, where the horizontal and vertical polarization contributions are balanced. The CNOT operation succeeds with probability $P = \frac{1}{9}$.

III. VARIATIONAL QUANTUM PROCESS TOMOGRAPHY

Let us consider the variational quantum tomography method for the characterization of the integrated CNOT gate. In general, a completely positive trace-preserving map $\mathcal{E}$ for a two-qubit process can be represented as

$$\mathcal{E}(\rho) = \sum_{i,j=1}^{16} \chi_{ij}\sigma_i\rho\sigma_j^\dagger, \tag{2}$$

where ρ is the system initial state, and $\{\sigma_i\}$ is the SU(4) basis, i.e., the Pauli matrices for two qubits. In particular, we choose σ_{16} as the identity, and the other operators are traceless matrices satisfying $\text{Tr}(\sigma_i\sigma_j) = 4\delta_{ij}$ $(i,j < 16)$. The χ_{ij} defines the superoperator χ, containing all the information dealing with the process. It is a normalized Hermitian positive semidefinite operator.

TABLE I. Sequence of 16 pure polarization states used to characterize the gate in the experiment. The product of a line and a column defines a state. For instance, $|\text{RL}\rangle$ is the seventh state. The polarizations are horizontal (H), vertical (V), circular left (L), circular right (R), diagonal (D), and antidiagonal (A).

	A	H	L	V
V	1	2	3	4
R	5	6	7	8
H	9	10	11	12
	A	H	R	V
D	13	14	15	16

In the CNOT gate the control qubit is encoded in the horizontal or vertical basis while the target is in the diagonal basis. If both target and control qubits are encoded in the vertical or horizontal polarization state, the circuit implements a controlled-Z (CZ) gate. For simplicity, in the following we consider the optical CZ gate (U) (the CNOT process matrix can be easily obtained by applying a rotation on the target qubit subspace). With vertical (V) and horizontal (H) polarizations defining the canonical basis,

$$|\text{V}\rangle = \begin{pmatrix} 1 \\ 0 \end{pmatrix}, \quad |\text{H}\rangle = \begin{pmatrix} 0 \\ 1 \end{pmatrix}, \tag{3}$$

the matrix representation of the gate is

$$U = \begin{pmatrix} 1 & 0 & 0 & 0 \\ 0 & 1 & 0 & 0 \\ 0 & 0 & 1 & 0 \\ 0 & 0 & 0 & -1 \end{pmatrix}. \tag{4}$$

Therefore, our gate corresponds to a Kraus rank-1 process with the following Kraus representation:

$$\mathcal{E}(\rho) = U\rho U^\dagger. \tag{5}$$

In the experiment, the gate is characterized by its action on the 16 distinct polarization pure states defined in Table I. After the action of the gate on a given input state ($U|i\rangle = |i_{\text{out}}\rangle$), the output state ($|i_{\text{out}}\rangle$) is characterized by the measurement of the 36 projectors listed in Table II.

TABLE II. Sequence of 36 projectors measured in the experiment. The product of a line and a column defines the projector. For instance, $|\text{DA}\rangle\langle\text{DA}|$ is the seventh projector. The polarizations are horizontal (H), vertical (V), circular left (L), circular right (R), diagonal (D), and antidiagonal (A).

	V	H	A	D	R	L
V	1	2	13	14	17	18
H	3	4	15	16	19	20
A	21	22	5	6	25	26
D	23	24	7	8	27	28
R	29	30	33	34	9	10
L	31	32	35	36	11	12

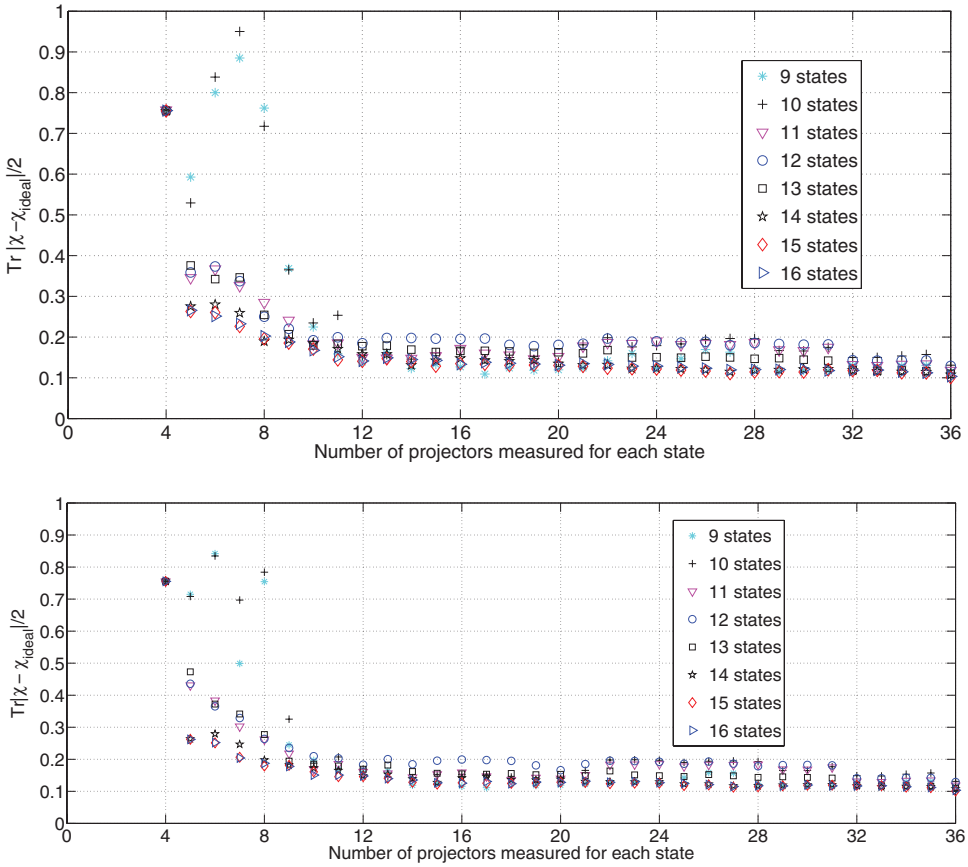

FIG. 2. (Color online) Convergence of the map (χ) reconstruction as the number of distinct measurements is increased. The figure of merit is the trace distance to the ideal map. In the top panel, the sequence of states used in the reconstruction is that of Table I, while in the bottom panel the sequence is reversed. One can see that the convergence does not depend on the sequence of states. The total number of distinct measurements in the experiment is 576 (16 states $\times$ 36 projectors). With just 12 projectors per state, the map reconstruction is already converged for the number of states varying from 9 to 16. Note that with just 108 distinct measurements (9 states $\times$ 12 projectors) the map is already reconstructed with high fidelity (see Table IV).

As previously mentioned, VQT allows for the reconstruction of the map with partial information. This means that we do not need to use all the states of Table I and all the projectors of Table II to reconstruct the map. Rather, from the total of 16 states and 36 projectors, we are able to reconstruct the map using $N_{\rm st}$ states ($N_{\rm st} \leqslant 16$) and $N_{\rm proj}$ projectors ($N_{\rm proj} \leqslant 36$). Hence, the possibility of using partial information in the process tomography can contribute to substantial savings in the experimental measurements. Furthermore, we are able to compare the maps reconstructed with different portions of the experimental data in order to gather relevant information about the very consistency of the data, or the stability of the experimental setup, and the quality of the device to characterize.

Let f_{mk} be the measured frequency for projection of the state $|k_{\rm in}\rangle$, from Table I, on the projector P_m, from Table II, after the action of the gate. The SDP outlined in Eq. (6) returns an optimal approximation (χ) for the map, using $N_{\rm st} \times N_{\rm proj}$ measured frequencies (f_{mk}). In the SDP we have the following unknowns: the map superoperator χ, built to be positive semidefinite ($\chi \geqslant 0$) and normalized [$\mathrm{Tr}(\chi) = 1$]; the output states $\varrho^k_{\rm out}$, which are constrained to be positive semidefinite ($\varrho^k_{\rm out} \geqslant 0$), but not necessarily pure or normalized [$\mathrm{Tr}(\varrho^k_{\rm out} \leqslant 1)$] because of the inherent experimental imprecisions; and finally the small positive parameters Δ_{mk}, accounting for deviations of the frequencies from probabilities, due once more to the inherent experimental imprecisions. What the program does is to determine valid χ and $\{\varrho^k_{\rm out}\}$, compatible with minimum disturbance on the measured frequencies, therefore the minimization over the $\{\Delta_{mk}\}$, and minimum values for the unmeasured projections [$\mathrm{Tr}(P_n \varrho^k_{\rm out})$ for $n > N_{\rm proj}$)].

$$\text{minimize} \left\{ \sum_{k=1}^{N_{\rm st}} \left[\sum_{m=1}^{N_{\rm proj}} \Delta_{mk} + \sum_{n=N_{\rm proj}+1}^{36} \mathrm{Tr}\left(P_n \varrho^k_{\rm out}\right) \right] \right\}$$

$$\text{subject to} \begin{cases} \chi \geqslant 0, \\ \mathrm{Tr}(\chi) = 1, \\ \varrho^k_{\rm out} \geqslant 0, \\ \mathrm{Tr}\left(\varrho^k_{\rm out}\right) \leqslant 1, \\ \varrho^k_{\rm out} = \sum_{i,j=1}^{16} \chi_{ij} \sigma_i |k_{\rm in}\rangle\langle k_{\rm in}| \sigma_j, \\ (1 - \Delta_{mk}) f_{mk} \leqslant \mathrm{Tr}\left(\varrho^k_{\rm out} P_m\right) \leqslant f_{mk}(1 + \Delta_{mk}), \\ \Delta_{mk} \geqslant 0, \\ \forall\, k \in [1, N_{\rm st}], \text{ and } \forall\, m \in [1, N_{\rm proj}]. \end{cases} \tag{6}$$

Table III shows what is expected if we had access to the output probabilities, i.e., if the measured frequencies coincided with $\langle k_{\rm out}|P_m|k_{\rm out}\rangle$. In this case, in order to recover the ideal map we need at least 9 states. In this ideal scenario, the best strategy would be 11 states and 5 projectors, which amounts to just 55 distinct measurements instead of the 256 employed in the previously reported standard QPT [20].

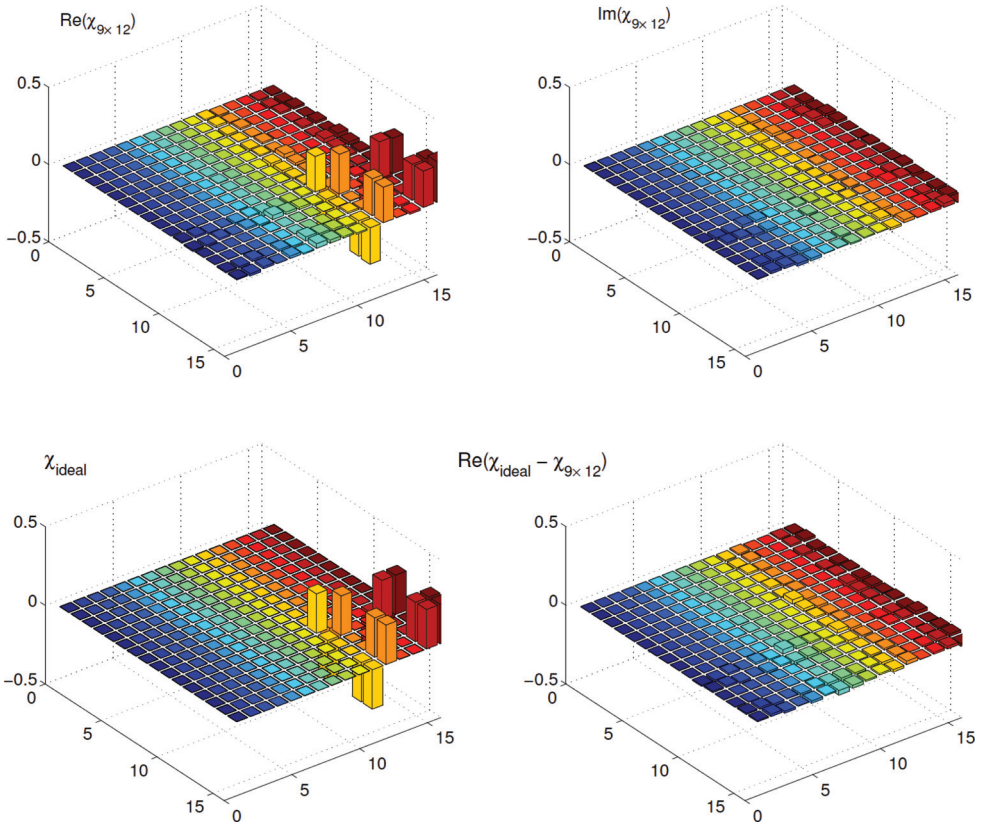

FIG. 3. (Color online) Reconstructed map with 9 states and 12 projectors per state. (Top) Real part of the reconstructed map (left) and the imaginary part (right). (Bottom) Ideal map (left) and the difference between the real parts of ideal and reconstructed maps (right).

IV. EXPERIMENTAL VQT OF CZ GATE

We briefly review the experimental apparatus adopted in Ref. [20] (see Fig. 1): Photon pairs are generated via spontaneous parametric down-conversion in a nonlinear crystal; their polarization state is prepared in any of the states reported in Table I by means of wave plates and polarizing beam splitters. Photon pairs are then delivered through single-mode fibers to the integrated CZ gate for polarization qubits realized by the ultrafast laser writing technique [30]. Finally, state tomography of the outcoming photons is performed with standard polarization analysis setups. While in Ref. [20] all the measurements required for a standard QPT were performed and the process matrix $\chi_{i,j}$ was reconstructed by following the standard QPT approach, here we make use of a partial set of those experimental data to obtain the same process matrix by means of the VQT method.

Figure 2 shows the reconstruction of the map with the experimental data. As a figure of merit we use the trace distance of the reconstructed map to the ideal one, $\mathrm{Tr}|\chi - \chi_{\mathrm{ideal}}|/2$, as a function of the number of projectors measured for each input state. In the top panel, the sequence of states is that of Table I, while in the bottom panel the sequence is reversed. Note the quasimonotonic convergence of the reconstruction as the number of distinct measurements increases. Comparing the two panels, one can see that different portions of the experimental data can be used to reconstruct the map with high fidelity. Using 12 projectors per state, the reconstruction converges for any number of states, and the inclusion of additional experimental data does not affect the convergence. These results testify that the photonic quantum gate is stable

TABLE III. Minimum number of projectors necessary to reconstruct the map with a precision of $\frac{1}{2}\mathrm{Tr}|\chi - \chi_{\mathrm{ideal}}| < 10^{-4}$, in the case of perfect measurements. The table is obtained by running the program (6), with states and projectors chosen in the sequence given in Tables I and II. With less than 9 states it is not possible to reconstruct the map with a precision of less than 0.5 in the trace distance.

No. of states	Minimum No. of projectors
9	25
10	9
11	5
12	5
13	5
14	5
15	5
16	5

TABLE IV. Process fidelities for the reconstructed maps with respect to the ideal map, with different sets of input states and projectors. The table highlights the quality of the tomography reconstruction shown in Fig. 2. Uncertainties arise from the Poisson distribution of counting statistics.

No. of states	No. of projectors	Fidelity
9	12	0.9514
10	12	0.9569
13	12	0.9684
16	36	0.9762

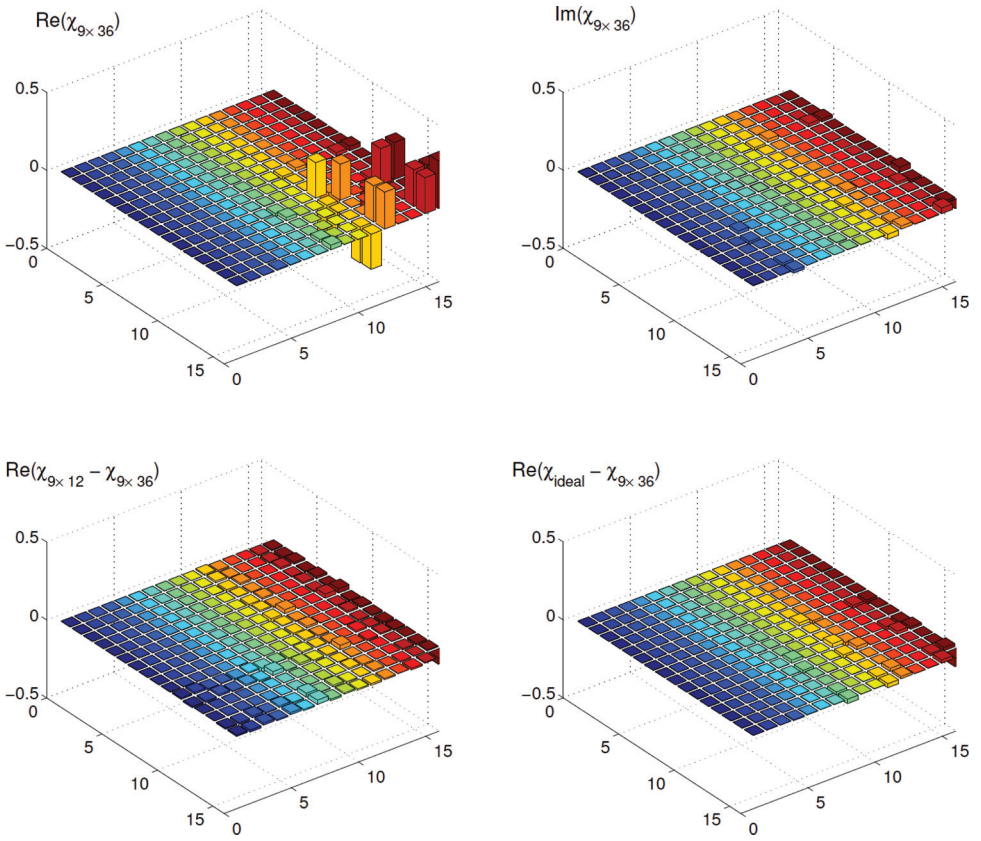

FIG. 4. (Color online) Reconstructed map with 9 states and 36 projectors per state. (Top) Real part of the reconstructed map (left) and the imaginary part (right). (Bottom) Difference of reconstructed maps with 12 and 36 projectors (left) and the difference between the ideal and reconstructed maps (right).

and operates with high fidelity for all states in an indiscriminate way. Figures 3 to 6 compare the maps with the minimum (9) and maximum (16) number of states and 12 and 36 projectors. One can see that there is no relevant difference among the

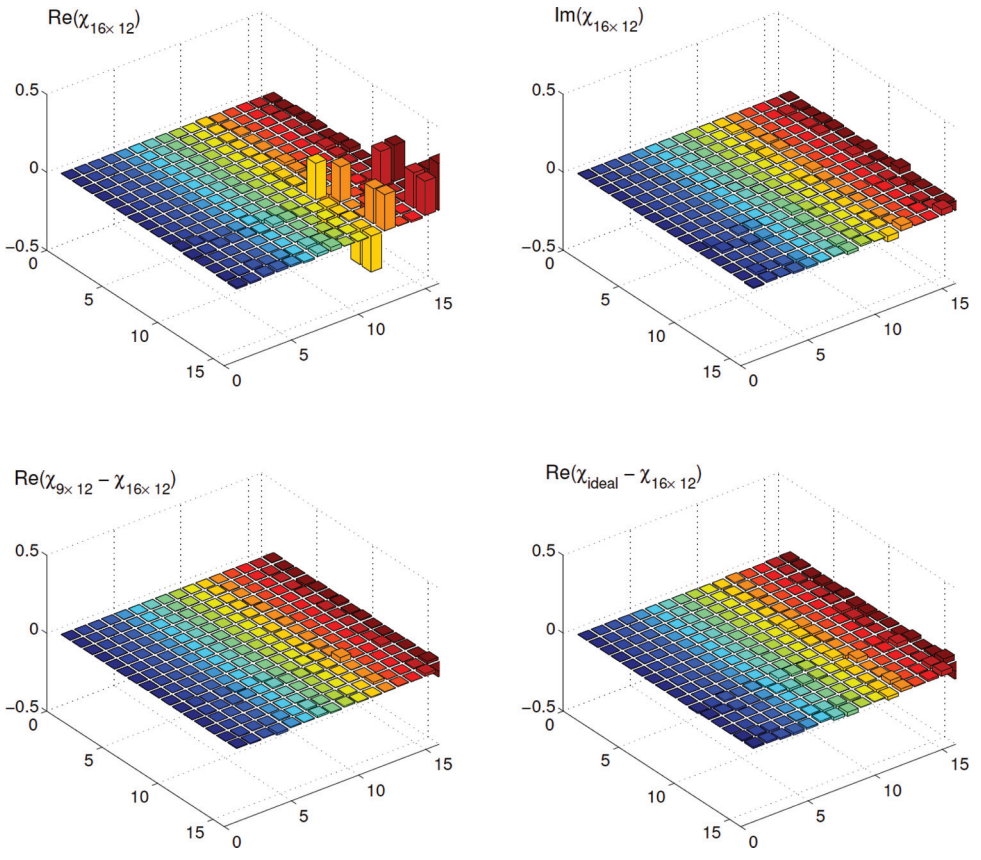

FIG. 5. (Color online) Reconstructed map with 16 states and 12 projectors per state. (Top) Real part of the reconstructed map (left) and the imaginary part (right). (Bottom) Difference of reconstructed maps with 9 and 16 states (left) and the difference between ideal and reconstructed maps (right).

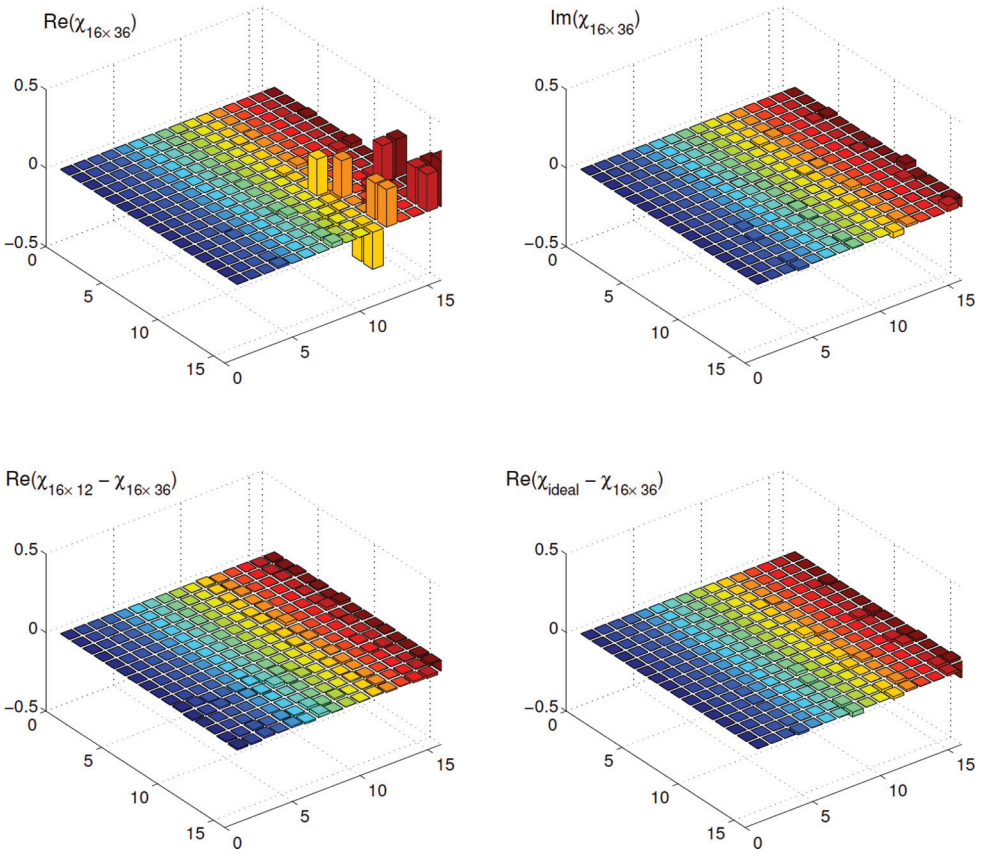

FIG. 6. (Color online) Reconstructed map with 16 states and 36 projectors per state. (Top) Real part of the reconstructed map (left) and the imaginary part (right). (Bottom) Difference of reconstructed maps with 12 and 36 projectors (left) and the difference between ideal and reconstructed maps (right).

maps. It is a signature of the consistency and quality of measurements and the stability of the photonic quantum gate.

In order to validate the above results, we also calculated the process fidelities [3] (i.e., the analogous of quantum state

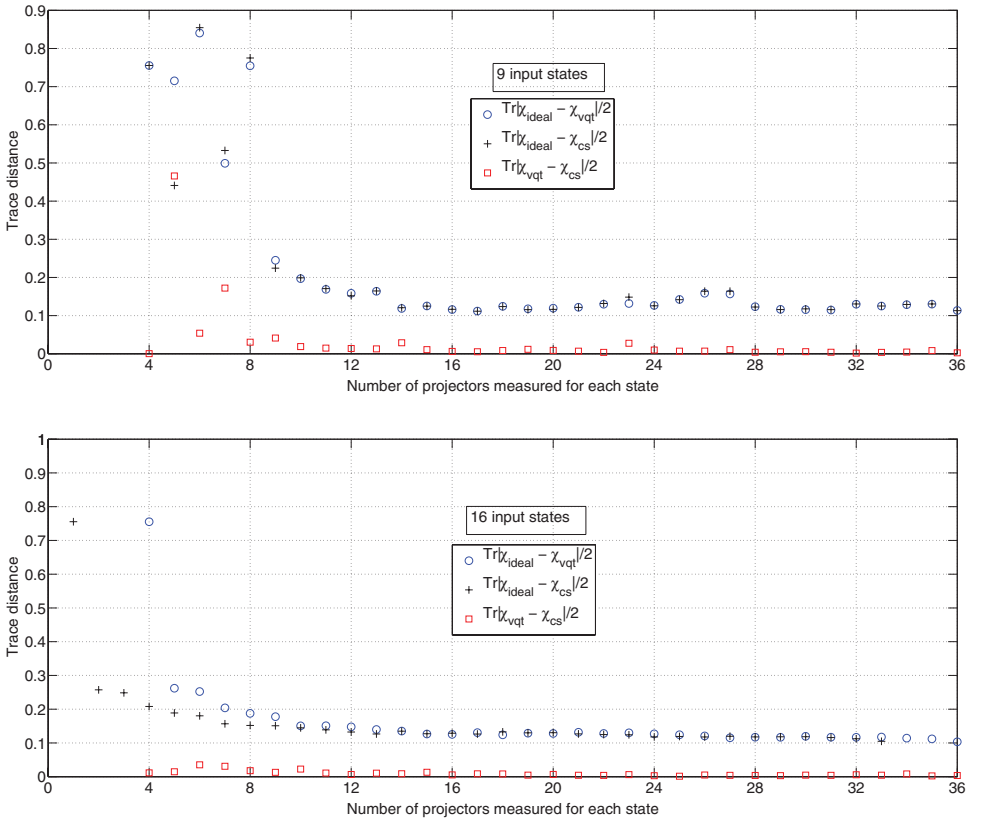

FIG. 7. (Color online) Convergence of the map (χ) reconstruction as the number of distinct measurements is increased, using compressed sensing [Eq. (8)] and VQT [Eq. (6)]. The figure of merit is the trace distance to the ideal map. We also plot the trace distance between the maps obtained via VQT and CS. It is clearly shown that the methods are completely equivalent, converging with the same cost. In the top panel, we used the minimum number of states (9) to have a high-fidelity reconstruction. In the bottom panel, we used all the states (16) available.

fidelity [31] for two processes),

$$\Delta = \frac{\mathrm{Tr}[\sqrt{\sqrt{\chi}\,\chi_{id}\sqrt{\chi}}]^2}{\mathrm{Tr}[\chi]\mathrm{Tr}[\chi_{id}]}, \tag{7}$$

between the theoretical map χ_{id} and the maps χ obtained by VQT with different sets of states and projectors. The obtained values are reported in Table IV. We can observe that the map obtained with 9 states and 12 projectors already presents a process fidelity that approaches the maximum value achievable with this experimental setup.

We finish this section comparing our approach (VQT) with compressed sensing (CS) tomographies [5,8]. While in VQT we minimize the projections over unmeasured projectors [viz. first line of Eq. (6)], in CS one has to minimize the nuclear norm, or l_1 norm, of the state being reconstructed. Therefore, we can come out with a CS version of process tomography by modifying the first line of Eq. (6). The new algorithm reads

$$\text{minimize} \sum_{k=1}^{N_{\mathrm{st}}} \left[\left|\left|\varrho^k_{\mathrm{out}}\right|\right|_{l_1} + \sum_{m=1}^{N_{\mathrm{proj}}} \Delta_{mk} \right]. \tag{8}$$

Note that the minimization is done under the same constraints of Eq. (6). In Fig. 7 the two methods are compared. The two methods are clearly equivalent, converging with the same cost and with the same fidelities. Both methods are a viable alternative to circumvent the exponential growth of the parameters in the Hilbert space, when the state or process to be reconstructed is of low rank.

V. CONCLUSION

We have performed a QPT analysis of the first integrated photonic two-qubit gate for polarization qubits, using the new VQT method. This benchmark study shows, on one hand, the efficiency of the method and, on the other hand, the stability and robustness of the photonic two-qubit gate. The possibility of using partial information in the process tomography, allied to the computational efficiency with which linear convex optimization problems can be solved, makes VQT promising for the study of quantum processes of many qubits.

ACKNOWLEDGMENTS

We acknowledge financial support from the Brazilian CNR-CNPq cooperation project, FAPEMIG, and INCT-IQ (National Institute of Science and Technology for Quantum Information) and from EU-Project CHISTERA-QUASAR, FIRB-Futuro in Ricerca HYTEQ, PRIN 2009, and ERC-Starting Grant 3D-QUEST (3D-Quantum Integrated Optical Simulation).

[1] M. Mohseni, A. T. Rezakhani, and D. A. Lidar, Phys. Rev. A **77**, 032322 (2008).
[2] I. L. Chuang and M. A. Nielsen, J. Mod. Opt. **44**, 2455 (1997).
[3] I. Bongioanni, L. Sansoni, F. Sciarrino, G. Vallone, and P. Mataloni, Phys. Rev. A **82**, 042307 (2010).
[4] M. Silva, E. Magesan, D. W. Kribs, and J. Emerson, Phys. Rev. A **78**, 012347 (2008).
[5] D. Gross, Y. Liu, S. T. Flammia, S. Becker, and J. Eisert, Phys. Rev. Lett. **105**, 150401 (2010).
[6] A. Bendersky, F. Pastawski, and J. P. Paz, Phys. Rev. A **80**, 032116 (2009).
[7] M. Cramer, M. B. Plenio, S. T. Flammia, R. Somma, D. Gross, S. D. Bartlett, O. Landon-Cardinal, D. Poulin, and Y. Liu, Nat. Commun. **1**, 149 (2010).
[8] A. Shabani, R. L. Kosut, M. Mohseni, H. Rabitz, M. A. Broome, M. P. Almeida, A. Fedrizzi, and A. G. White, Phys. Rev. Lett. **106**, 100401 (2011).
[9] W. Liu, T. Zhang, J. Liu, P. Chen, and J. Yuan, Phys. Rev. Lett. **108**, 170403 (2012).
[10] S. T. Flammia and Y. Liu, Phys. Rev. Lett. **106**, 230501 (2011).
[11] J. O. S. Yin and S. J. van Enk, Phys. Rev. A **83**, 062110 (2011).
[12] T. O. Maciel and R. O. Vianna, Quantum Inf. Comput. **12**, 0442 (2012).
[13] T. O. Maciel, A. T. Cesário, and R. O. Vianna, Int. J. Mod. Phys. C **22**, 1361 (2011).
[14] S. Boyd and L. Vandenberghe, *Convex Optimization* (Cambridge University Press, Cambridge, 2000).
[15] J. F. Sturm, Optim. Methods Software **11**, 625 (1999), Special issue on Interior Point Methods (CD supplement with software); SEDUMI http://fewcal.kub.nl/sturm/softwares/sedumi.html; J. Lö fberg, *YALMIP : A Toolbox for Modeling and Optimization in MATLAB, Proceedings of the CACSD Conference, 2004, Taipei, Taiwan* (unpublished), http://control.ee.ethz.ch/~joloef/yalmip.php.
[16] E. Jaynes, Phys. Rev. **106**, 620 (1957).
[17] V. Buzek, Lect. Notes Phys. **649**, 189 (2004).
[18] G. Lima, E. S. Gómez, A. Vargas, R. O. Vianna, and C. Saavedra, Phys. Rev. A **82**, 012302 (2010).
[19] J. G. Filgueiras, T. O. Maciel, R. E. Auccaise, R. O. Vianna, R. S. Sarthour, and I. S. Oliveira, Quantum Inf. Proc. **11**, 1883 (2012).
[20] A. Crespi, R. Ramponi, R. Osellame, L. Sansoni, I. Bongioanni, F. Sciarrino, G. Vallone, and P. Mataloni, Nat. Commun. **2**, 566 (2011).
[21] I. L. Chuang and M. A. Nielsen, *Quantum Information and Quantum Computation* (Cambridge University Press, Cambridge, 2000).
[22] T. Ralph, N. K. Langford, T. Bell, and A. G. White, Phys. Rev. A **65**, 062324 (2002).
[23] H. F. Hofmann and S. Takeuchi, Phys. Rev. A **66**, 024308 (2002).
[24] C. K. Hong, Z. Y. Ou, and L. Mandel, Phys. Rev. Lett. **59**, 2044 (1987).
[25] J. L. O'Brien, G. J. Pryde, A. G. White, T. C. Ralph, and D. Branning, Nature (London) **426**, 264 (2003).
[26] N. Kiesel, C. Schmid, U. Weber, R. Ursin, and H. Weinfurter, Phys. Rev. Lett. **95**, 210505 (2005).

[27] R. Okamoto, H. F. Hofmann, S. Takeuchi, and K. Sasaki, Phys. Rev. Lett. **95**, 210506 (2005).

[28] N. K. Langford, T. J. Weinhold, R. Prevedel, K. J. Resch, A. Gilchrist, J. L. O'Brien, G. J. Pryde, and A. G. White, Phys. Rev. Lett. **95**, 210504 (2005).

[29] A. S. Clark, J. Fulconis, J. G. Rarity, W. J. Wadsworth, and J. L. O'Brien, Phys. Rev. A **79**, 030303(R) (2009).

[30] L. Sansoni, F. Sciarrino, G. Vallone, P. Mataloni, A. Crespi, R. Ramponi, and R. Osellame, Phys. Rev. Lett. **105**, 200503 (2010).

[31] R. Jozsa, J. Mod. Opt. **41**, 2315 (1994).